JOURNAL OF DEGRADED AND MINING LANDS MANAGEMENT
Volume 10, Number 2 (January 2023):4047-4059, doi:10.15243/jdmlm.2023.102.4047
ISSN: 2339-076X (p); 2502-2458 (e), www.jdmlm.ub.ac.id

Research Article

Land subsidence assessment on karst based on resistivity and geotechnical parameters

Muhammad Altin Massinai*, Muhammad Fawzy Ismullah Massinai, Erfan Syamsuddin

Department of Geophysics, Faculty of Mathematics and Natural Sciences, Hasanuddin University, Makassar, 90245, Indonesia

*corresponding author: altin@science.unhas.ac.id

Article history:
Received 20 August 2022
Accepted 12 October 2022
Published 1 January 2023

Keywords:
cavities
landslide
limestone
soil
water

Abstract

Karst is geomorphologically composed of limestone. However, limestone is very susceptible to weathering due to the influence of water, which can cause land subsidence. The resistivity method is often used to determine the potential for land subsidence, while geotechnical methods are commonly considered capable of juxtaposing with resistivity methods to support interpretation accuracy. The current research was conducted to determine the potential for land subsidence in the karst area in Lappae, South Sulawesi, Indonesia. The resistivity method utilizes a dipole-dipole configuration, and the geotechnical parameters used are uniformity coefficient, curvature coefficient, water content, shear angle, and cohesion. The results obtained can be classified into northern and southern areas. The classification of these areas is based on the resistivity results, which show very high resistivity values (> 4800 Ωm) in the southern part. This value is assumed to be a feature of the cave. Caves are predominantly distributed in the southern part. The five geotechnical parameters show that the northern part, which was composed of massive limestone (150-1600 Ωm), is a stable area, though it is highly prone to landslides. As for the southern part, geotechnical parameters suggest that the presence of caves is the primary factor contributing to the very high potential for landslides in this region. These results indicate that, based on the evaluation of this location, it is not feasible for land use. In addition, in spite of the low cost and rapid methods, the combination of these methods shows good results.

To cite this article: Massinai, M.A., Massinai, M.F.I. and Syamsuddin, E. 2023. Land subsidence assessment on karst based on resistivity and geotechnical parameters. Journal of Degraded and Mining Lands Management 10(2):4047-4059, doi:10.15243/jdmlm.2023.102.4047.

Introduction

Karst area is a unique geomorphological area, especially in regard to land use. Karst structures can pose threats to buildings, agriculture, transportation facilities, and others. Hypothetically, this threat could be the result of the slow migration of fine particles that causes the compaction process to fail and bring disasters, such as land subsidence and collapse (Bakhshipour et al., 2013; Ezersky et al., 2017). Land subsidence is related to the existence of caves. Caves can be defined as the expansion of pores in carbonate rocks, such as limestone and dolomite, due to weathering and the development of the karst itself by groundwater (Baluch et al., 2022). The soil surface will become unstable if the rock conditions below the surface experience weathering (Massinai and Massinai, 2018; Massinai et al., 2019; García-Soriano et al., 2020). Factors that could serve as indicators in determining the strength of the ground are the thickness of the surface layer, the physical condition of the soil, and subsurface rocks (Figueroa-Miranda et al., 2018; Ikuemonisan and Ozebo, 2020). Therefore, the

karst cavity can potentially pose threats, as mentioned above. The main problem, in this case, is finding out the cavity in the karst area as it is difficult to predict, while it has the potential to cause a geohazard. The method that can be expected to address this problem is the geophysical method. Geophysical methods are considered highly effective for geohazard investigations due to their non-intrusive nature and cost-effectiveness. Geophysical methods can provide a cost-effective solution for investigating the subsurface and precisely detecting a karst cavity (Bakhshipour et al., 2013). A geophysical method that has been developed to detect cavities in the last few decades is the resistivity method. This method utilizes electricity in the subsurface. The resistivity method provides a fast and cost-effective alternative for identifying shallow subsurface conditions with an acceptable result. Research on caves using the resistivity method has been carried out in many different sites beyond Indonesia, such as in Yongweol-Ri, South Korea (Farooq et al., 2012), in Riyadh, KSA (Abd El Aal, 2017), and Goronyo Dam, Nigeria (Augie et al., 2022).

Geophysical methods can offer results that are not unique, which is commonly referred to as ambiguity, in which results obtained are less accurate. The ambiguity associated with interpretation makes most single geophysical methods imprecise (Arisona et al., 2020). To address this issue, we offer a geotechnical method. Several studies have been conducted combining geophysics and geotechnical research (Arisona et al., 2020; Baluch et al., 2022; Wilopo et al., 2022). In this study, geotechnical methods were employed to determine soil resistance from various stresses that would possibly arise. That is to say that the geotechnical method was used to complement geophysical methods.

This research attempted to establish a relationship between resistivity value and several coefficients in a geotechnical site investigation to identify caves and prone-zone to subsidence/ landslide. This research is expected to contribute ideas and make new insights into scientific development using resistivity and geotechnical methods. The combination of the two methods is considered very suitable for infrastructure development. This research can benefit the community, government, and private sector by providing information about sinking-prone zones. This research directly provides a potential contribution to the government to guarantee the population's comfort and safe feeling, especially for residents and housing infrastructure, particularly in the research area.

Methods

Research area

The research was conducted in Lappae, Bone, South Sulawesi, Indonesia. Lappae is located at coordinates 4°21'52" S - 4°24'10" S and 120°11'56" - 120°13'52" E Longitude. This area is geologically located in Taccipi Formation. The Taccipi Formation and the Walane Formation are located in South Sulawesi. The Walanae Fault separates the two formations. The Walanae Formation is not locally aligned with the Taccipi Formation. The Walanae Formation is late Miocene to Pliocene, while the Taccipi Formation is mid-Miocene to Pliocene (Massinai et al., 2014). Limestone in the Taccipi Formation (Imran et al., 2016) intersects with the Walanae Formation, consisting of calcareous mudstone and arenaceous (Pusparini et al., 2019). In Lappae, Taccipi Formation consists of alluvium, and limestone (grain-stone), as shown in Figure 1. In the area of the Taccipi Formation, there are many caves in the subsurface. Two of the cave's entrances are found in the Taccipi Formation, located in the Lappae area, Bone Regency, South Sulawesi, Indonesia. One of them is around 2 m in height (Figure 2). The cave in limestone is one of the characteristics of karst morphology.

The geomorphological condition of South Sulawesi, especially the Lappae area, Bone Regency, has unique characteristics. The beautiful topography in the form of hills is in great demand by real estate developers and the local community to be used as a residential location and agricultural activity (Figure 3, left). However, such topographical conditions require an in-depth study to convert into a settlement area. This condition makes this area prone to subsidence. Caves below the subsurface at this location with ample space are the product of tectonic activities (Farooq et al., 2012; Abd El Aal, 2017). As we had a conversation with local residents in this location, and they reported the land subsidence around their house (Figure 3, right).

Data acquisition and processing

The current study was conducted using resistivity and geotechnical methods. The resistivity measurement is generally carried out by injecting current into the ground through two current electrodes and measuring the potential difference between the two potential electrodes. The resistivity method analyses the subsurface based totally on the resistivity value in the 2D resistivity section. The space between the electrodes relies upon the resolution and depth of the desired object. Theoretically, the longer the space between the electrodes, the smaller the resolution, and the deeper the interpretation (Wilopo et al., 2022). Data retrieval was commenced by creating six measurement lines (L1-L6), as shown in Figure 4. The measurement line was created at a length of 300 m and a space between the electrodes of 5 m. The configuration used was the Dipole-dipole configuration. By using this configuration, it was assumed that a more precise subsurface cavity description could be yielded rather than using other types of electrode arrays (Farooq et al., 2012).

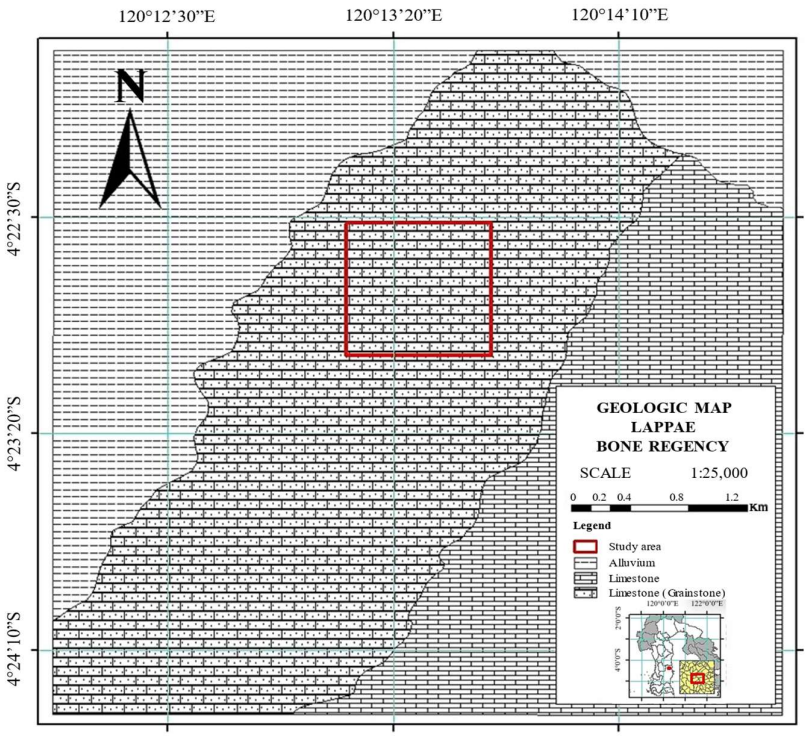

Figure 1. Geological map of the research area.

Figure 2. Two of the cave's entrances. (Right) The cave is around 2 m in height.

Figure 3. (Left) Rice field in the location. The sign of Lappae is inclined to the right, presumably due to land subsidence. (Right) Local residents reported land subsidence occurring behind their houses. The sign of land subsidence looked is visible in the cliff.

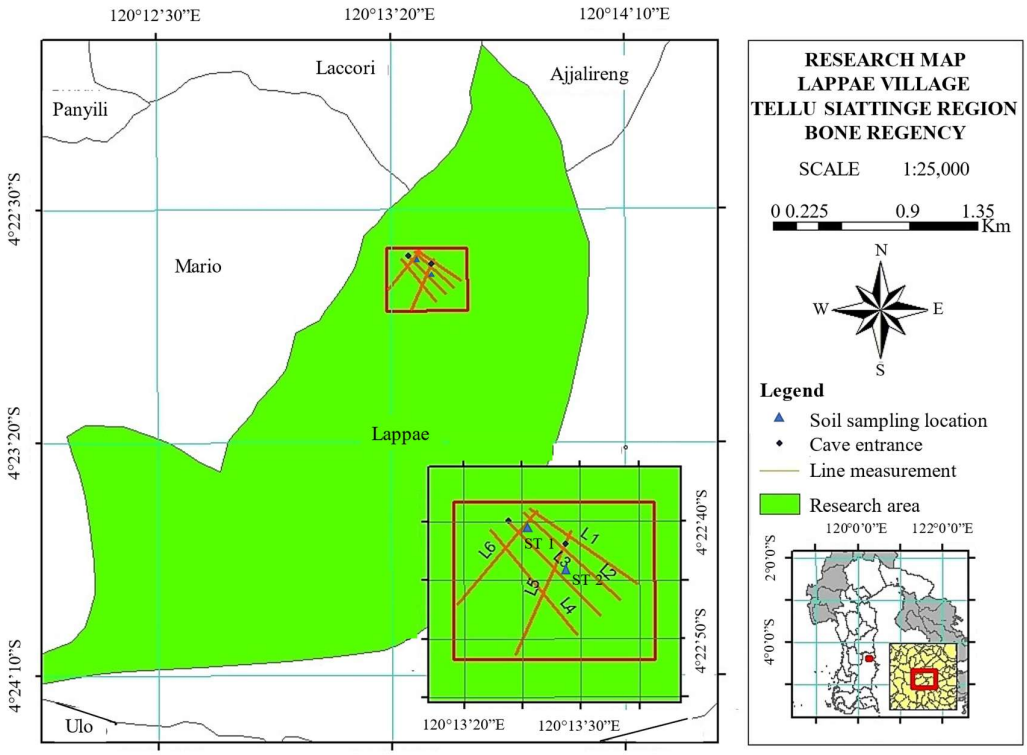

Figure 4. Map with the location of the resistivity measurement lines, soil sampling locations, and cave's entrance.

Observational data obtained from the measurement results were the value of current (I), potential difference (V), and spacing (n). Using this data, calculations were then carried out to determine the value of the geometry factor (K) and resistivity (ρ), so that the apparent resistivity (ρ) value could be obtained (Sari et al., 2019). The value was used to model the subsurface in 2D resistivity section, which contains the distribution of apparent resistivity values represented by different colors. Thus, qualitative data analysis was carried out on a 2D resistivity section. A cross-section of the subsurface cave and the thickness of the soil layer above would be obtained.

In geotechnical methods, we focus on five physical properties such as uniformity coefficient, curvature coefficient, water content, shear angle, and cohesion. The uniformity and curvature coefficients were obtained from sieve analysis. The properties of a particular type of soil depend on the grain size, which serves as the basis for classifying certain types of soil. Soil grain size is depicted on a graph, which is used as a gradation curve graph or a grain division curve graph. Soil that has a grain size distribution curve that is almost vertical (all particles are nearly the same size) is called uniform soil. If the curve extends over a rather large area, the soil is considered to be well-graded. The distinction between uniform and well-graded soils can be determined numerically by the uniformity coefficient (C_U) and curvature coefficient (C_C). The uniformity coefficient (C_U) and curvature coefficient (C_C) are usually used in the geotechnical field. These two coefficients are used as characteristic parameters to evaluate the grain composition of granular materials. The uniformity coefficient (C_U) indicates the uniformity distribution in the granular material, while the curvature coefficient (C_C) indicates an accumulation curve of grain composition gradation (Chen et al., 2018). Both of them are obtained from the interpretation of the grain size distribution curve. Soils with CU less than 4 are regarded as uniform soils, and soils with CU greater than 4 (6 for sand) are well-graded soils, as long as the grain size distribution curve is smooth and fairly symmetrical. The concavity coefficient CC is a measure of the symmetry and shape of the gradient curve. For well-graded soils, CC is between 1 and 3 (Das, 2021).

As regards water content, it is the ratio between water mass and dry soil mass expressed in %. In general, it can be assumed that the more saturated the soil with water, the higher the weathering rate, implying the greater the possibility of the occurrence of land subsidence (Das, 2021). Soil shear strength can be determined based on several geotechnical parameters, some of which are cohesion and shear angle. Shear angle (φ) and cohesion are two important physical properties of soil to determine the condition of slope material stability. Cohesion (C) is the attraction between similar particles that gives an

estimate of the strength of the material, in this case, the soil. Cohesion is not directly related to the laws of friction between material particles (Sujit, 2015).

Soil sampling was carried out in the research area. Observation of this slope was conducted from two different locations, i.e., Station 1 (ST 1) and Station 2 (ST 2). The samples were collected along with the resistivity measurement lines, while also considering the location of the cave's entrance. In the Soil Mechanics laboratory, the soil samples were heated before they were examined for their physical properties. The data acquisition process for both resistivity and geotechnical data can be seen in Figure 5.

Figure 5. (Left) Resistivity survey equipment. (Right) Soil sampling process.

Results and Discussion

Interpretation of 2D resistivity section

After carrying out the data acquisition process in the field, data loading for each line was conducted. The inversion results produce a 2D apparent resistivity section model that shows the depth and distribution of the apparent resistivity. We combined Line 1 (Figure 6), Line 2 (Figure 7), and Line 6 (Figure 8) were combined for interpretation. The results show that they seemed likely to have a similar pattern. Line 1 is parallel with Line 2, and they have a Southeast-Northwest orientation. Line 6 lies on the Northeast-Southwest orientation, and the line cuts Line 1 and Line 2 in the Northern part of the research area. We showed possible interpretations in four categories: aquifer layer, massive limestone, weathered limestone, and air-filled weathered limestone. The aquifer layer has 50-150 Ωm and lies on the deepest layer in Line 1, Line 2, and Line 6. This layer shows the possibility of clay with groundwater accumulation in their porous (Arisona et al., 2020). The second category is massive limestone. The layer is signed by 150-1600 Ωm and interpreted as a hard rock (Wilopo et al., 2022) in limestone formation. In Line 1, it lies at a depth of 50 – 80 m from the bottom. It is thicker on the next line, at a depth of 30 – 80 m, but in Line 6, it lies at a depth of 40 – 70 m from the bottom. When rainfall and water on the surface infiltrates the subsurface through the fracture, the infiltration increases the unconsolidated limestone condition and make the weathered limestone layer (Bakhshipour et al., 2013). It means that weathered limestone can possibly be located inside the massive limestone. We observed weathered limestone as the third category in Line 1, Line 2, and, Line 6. This category has 1600-4800 Ωm, and in Line 1 its shape is a boulder. In line 2, the weathered limestone has an irregular size. The limestone in Line 6 is in a big size, which is around 20 m in length and about 10 m thick. In the weathered layer, the water fills the porous and the fracture, and it makes them larger. When it is filled with air, it creates a cavity, void, or sinkhole. The resistivity layer with > 4800 Ωm indicates the presence of air-filled weathered limestone because it has a very high resistivity value. Generally, the detection of sinkhole sites is based on their high resistivity value (Ezersky et al., 2017). The sinkhole was apparent in Line 1 and Line 2 as a small cavity, which is not connected. However, in Line 6, the porous in the weathered layer is connected by fracture, and it looks like a huge and long cavity.

Another interesting object is the possibility of a land subsidence zone in these lines. Line 1 (150-160 m) and Line 2 (140-160 m) zones are not appropriate to be used as infrastructure or housing zone. Cave's entrance can be observed in Line 6, in a position of 30 m. Similarly, the zone between the cave's entrance to 120 m is not recommended to be used as a residential settlement. This condition is indicated by in the purple circle in Figures 6, 7, and 8. The limestone layer beneath that zone is a weathered zone with a very thin overburden layer. The area contains a limestone layer with cavities, which can possibly cause subsidence (Zhou et al., 2002). As Line 3 (Figure 9), Line 4 (Figure 10), and Line 5 (Figure 11) were analyzed, they can be interpreted as one part. Their resistivity section seemed to have a similar subsurface condition.

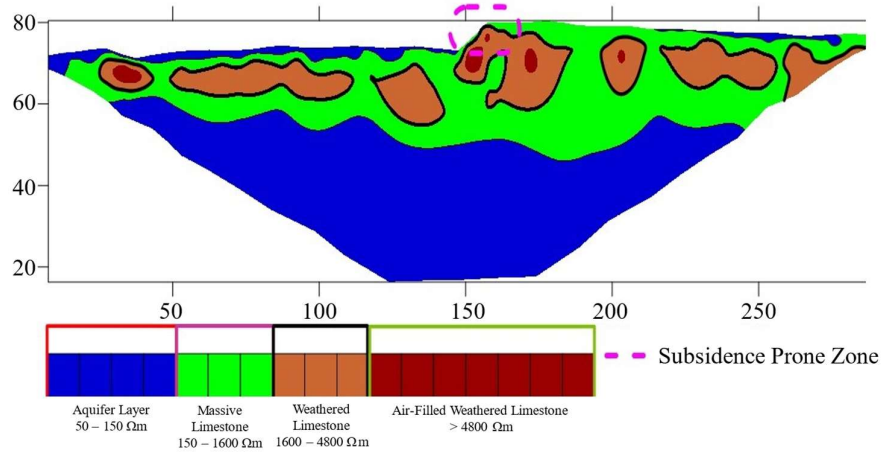

Figure 6. 2D apparent resistivity section interpretation of line 1.

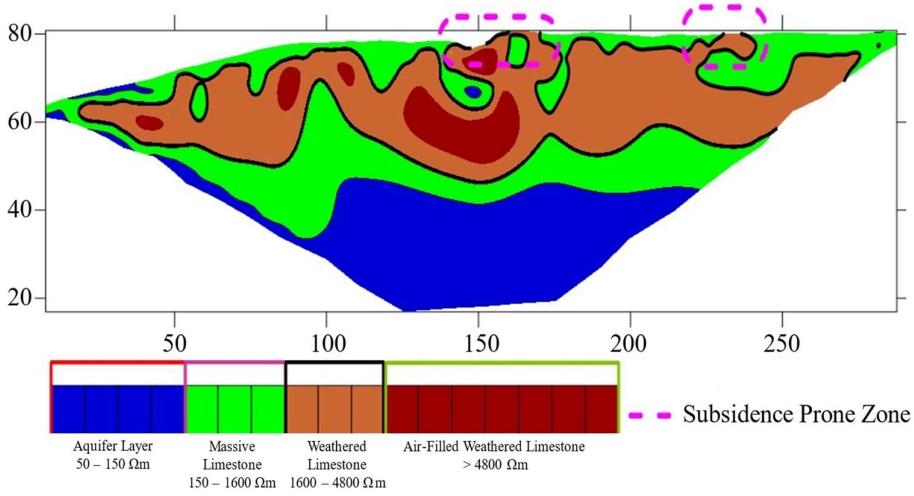

Figure 7. 2D apparent resistivity section interpretation of line 2.

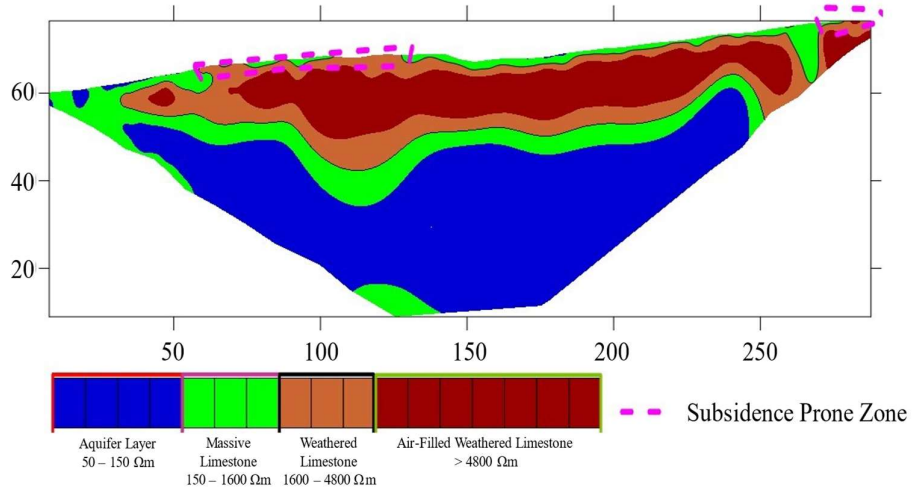

Figure 8. 2D apparent resistivity section interpretation of line 6.

Line 5 was Northeast-Southwest orientated, and it cuts Line 3 and Line 4 in the South of the research area. Line 3 and 4 are parallel with Line 1 and 2. The cave's entrance is located at the end of line 3. Overall, these three lines have 3 layers. The first layer is weathered limestone, which is indicated with resistivity >1600 Ωm. It is a very thick layer of about 70 m. Inside this layer, we found an anomaly with very high resistivity. It is highly weathered limestone with resistivity >4800 Ωm. The cavity is possibly formed by air in this layer because air has a very high resistivity value. In Line 3, air-filled weathered limestone has a large shape, but it is not connected well. The limestone height is around 10 m.

In Line 4 and 5, this cavity is connected to the Southern part of the research area. This fact supports our interpretation that a large cavity located in the southern area with dimensions are 10 m in height and around 50 m in length. The second layer that lies beneath weathered limestone is a massive limestone. This layer has a resistivity of 150-1600 Ωm, which is thinner than the previous layer, located at around 50 m depth from bedrock. The massive limestone was also observed in the northern part of the research area. Line 3,4, and 5 show the massive limestone as overburden with a thickness of about 1-2 m. At the deepest section lies the aquifer layer, which has the lowest resistivity of around 50-150 Ωm. After rainfall and surface water move through fractures in the weathered layer, the water fills the porous and makes a water table at that layer. This is called the aquifer layer. In Line 4 and 5, the aquifer layer is not connected, though in Line 3 the aquifer layer is connected. We believe that the aquifer layer still exists beneath this section.

Previously, we explained that the massive layer is located in the northern part of the research area, around 0-100 m. We can consider that this area is stable for building if the weathered layer is on the surface. The weathered layer has a cavity, void, or sinkhole inside. This condition is indicated with the purple circle in Figures 9, 10, and 11. Adding load over this layer could potentially cause a land subsidence zone in these areas. Cave's entrance was found in Line 3, in a position of 30 m. The weathered limestone layer with air-filled in its porous and fracture is a subsidence prone zone (Zhou et al., 2002).

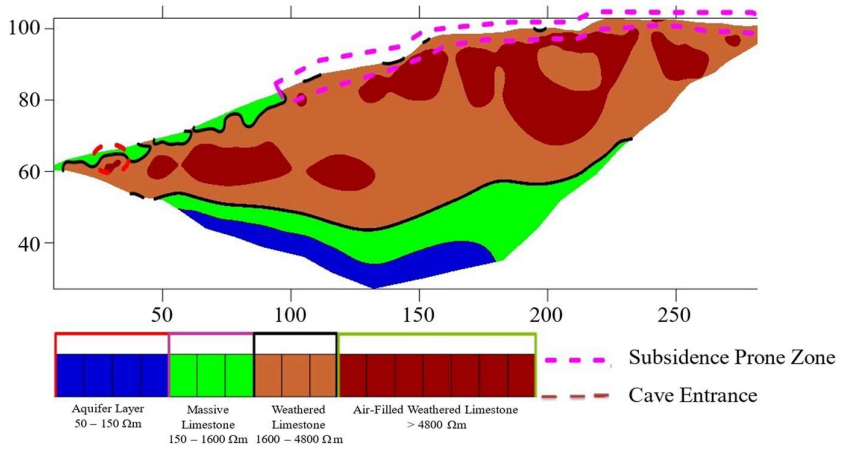

Figure 9. 2D apparent resistivity section interpretation of line 3.

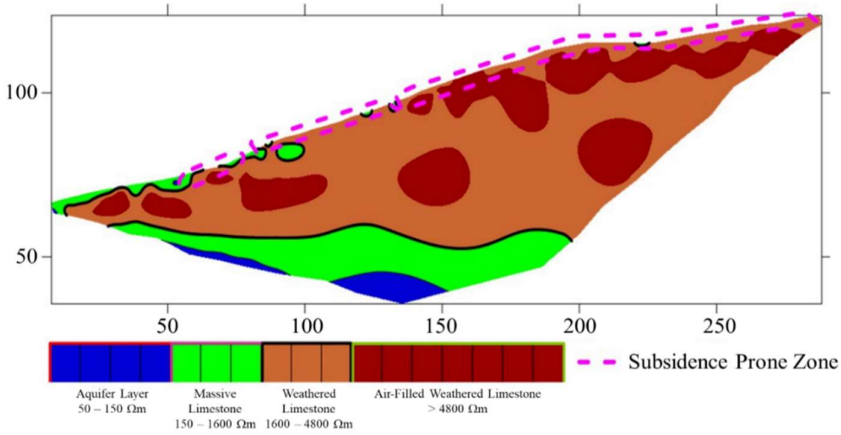

Figure 10. 2D apparent resistivity section interpretation of line 4.

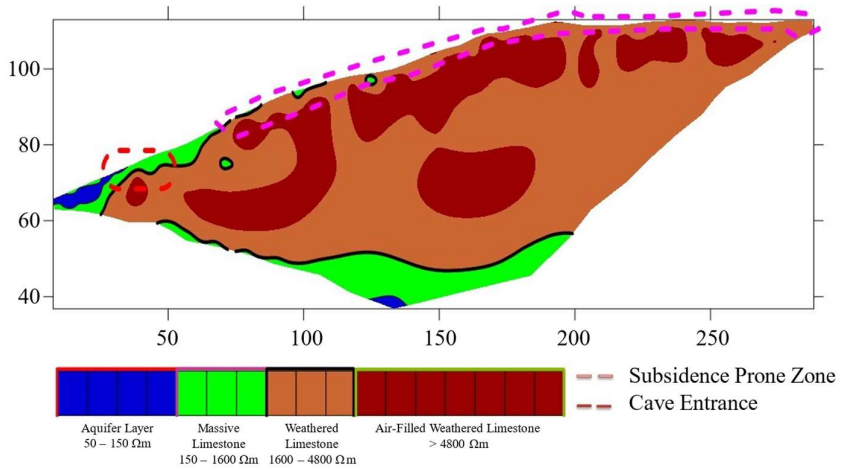

Figure 11. 2D apparent resistivity section interpretation of line 5.

Interpretation of 3D resistivity section

The 3D resistivity section is based on the 2D resistivity section of all lines. This section was created in order that we could be more focused on detecting voids in limestone karst in the study area. Based on this information, the distribution of cavities in the study area is shown in Figure 12.

This illustration clearly shows that the distribution of voids under the surface specifically happens in the southern part of the study area. In the 2D resistivity section Line 3 (Figure 9), Line 4 (Figure 10), and Line 5 (Figure 11) it can be seen that the southern part (more than 100 m) has a higher topography than the northern part (around 60 m). This fact indicates that if karstification develops, then the cavity will expand to the northern. Water, as the main control of the limestone grinding process, has been known to flow from a higher place to a lower place. When water enters the cavity in the southern part, of course, the water will erode down to the lower part, which is in the northern part. This process results in the expansion of the cavity in the northern part of the study area**.**

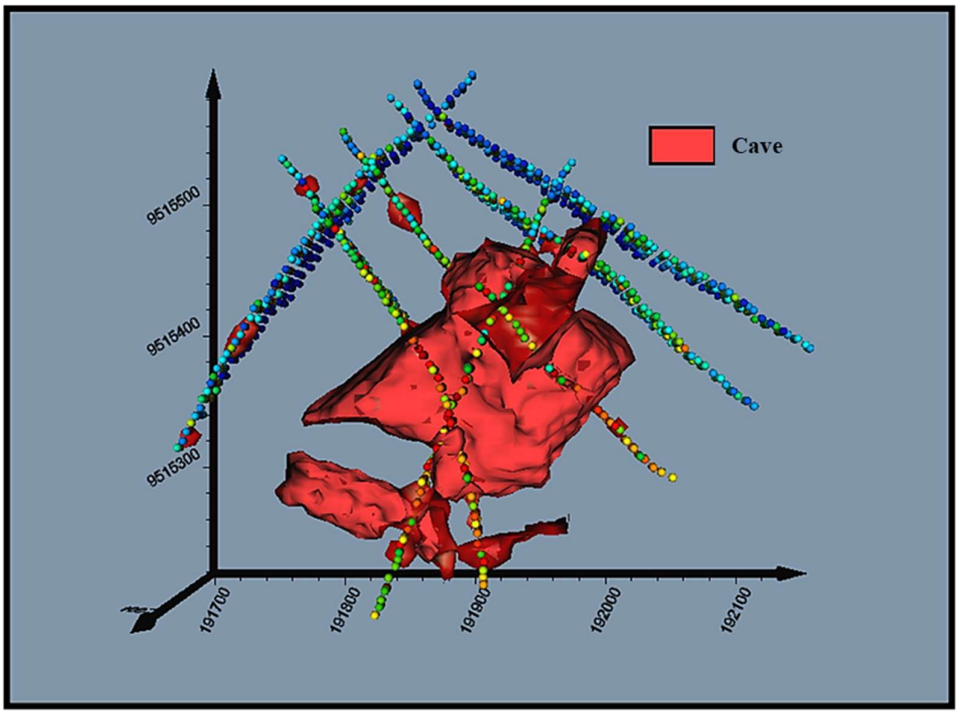

Figure 12. 3D apparent resistivity section.

Sieve analysis

Sieve analysis was carried out on soil samples taken at two points, i.e., ST 1 and ST 2. This location was chosen on the basis of the results of the previous 2D and 3D resistivity sections. The laboratory results show that the mass contents of ST 1 and ST 2 are at the same value of 1.8 kg/cm^3, which is categorized as low. At ST 1, the average density is 2.59 g/cm^3 in organic clay material. This organic clay is an uplift process in coral lithified into limestone (karst). While at ST 2, the average density is 2.67 g/cm^3 in coarse-sandy limestone material. Sieve analysis was carried out to determine the distribution of soil particle size (Oyeyemi et al., 2017). This process uses several types of sieves to separate sand, silt, and clay from each other based on their grain size. The portion retained on the sieve was weighed, and the percentage calculated as compared to the part that passed through the sieve**.** The sample at ST 1 is classified as sandy limestone. The percentage of granules that passes sieve no. 200 is 5.54%. The grain size of the soil at ST 1 consists of 5.54% of silt material and 94.46% of sandy limestone material. Regarding ST 2, which is coarse-grained soil with sandy limestone, the percentage of granules that passes sieve no. 200 is less than 5%. The grain size of the soil at ST 2 consists of 4.51% of silt material and 95.49% of sandy limestone material. Further results from this analysis can be seen in Table 1.

Figure 13 shows the sieve analysis graph as the input for the uniformity coefficient (C_U) and the curvature coefficient (C_C). The line of ST 1 shows the diameters of the grains that pass with the percentages of 10% (D10), 30% (D30), and 60% (D60) are 0.085, 0.273, and 0.721, respectively. Based on the grain size variation of the massive limestone, the C_U and C_C are 4.192 and 1.216, respectively. Sand has a C_U range of 1.5-8 (Wichtmann and Triantafyllidis, 2013). This sandy limestone is well-graded because the CC value is in the range of 1-3 (O'Kelly and Nogal, 2020).

Table 1. Results of soil sieve analysis.

Mesh diameter	ST 1		ST 2	
	% Retained	% Passing	% Retained	% Passing
4.75 mm (No. 4)	7.34	92.66	21.23	78.77
2.00 mm (No. 10)	17.36	82.64	46.40	53.60
1.015 mm (No. 18)	27.97	72.03	60.52	39.48
0.42 mm (No. 40)	48.06	51.94	76.17	23.83
0.25 mm (No. 60)	71.13	28.87	84.14	15.86
0.15 mm (No. 100)	82.98	17.02	91.61	8.39
0.0075 mm (No. 200)	94.46	5.54	95.49	4.51
Pan	100.00	0.00	100.00	0.00

At ST 2, the diameters of the grains that pass 10% (D10), 30% (D30), and 60% (D60) are 0.172, 0.655, and 2.704 respectively. Based on the value of the diameter of the grains of D10, D30, and D60, the C_U and C_C are 15.725 and 0.923, respectively. This C_U value is higher than the C_U of ST 1. Sand-gravel mixtures is found to have a C_U of around 15.9 (Wichtmann and Triantafyllidis, 2013), but this sand gravel is poor-graded because the CC value is less than 1 (O'Kelly and Nogal, 2020). ST 1 is located in the north, while ST 2 is in the south. Based on the cavities' position in the previous 3D resistivity section, it can be seen that ST 2 is located above the cave. The sample at ST 2 is interpreted as poorly graded sand gravel. The cave under ST 2 can be a filter. Particles above the cave tend to move in the cavity due to the effects of water seepage or vibration. Consequently, the filter only allows sand-sized grains to enter the cave. The sand continues to enter and fill the cave, which is caused by the gravity factor (ST 2 is higher than ST 1 topographically). The sand that accumulates in the northern area condenses and becomes soil, which is obtained at ST 1. The soil at ST 2 (the southern part of the study area) is considered to be internally unstable if it is characterized by larger particles (gravel) that are unable to block smaller particles (sand), which results in consequent layer erosion and fine particle erosion (Cortellazzo et al., 2021). The amount of soil particles also contributes to the discrepancy in resistivity values. In general, soil can take the form of both granular and fine particles, which also affects resistivity (Abidin et al., 2013). In this case, we can say that sandy limestone (ST 1) has a lower resistivity value than sand-gravel limestone (ST 2).

Water content analysis

The results of laboratory tests inform us that the average water content is 27.4% for ST 1 and 33.6% for ST 2 and these percentages are not significantly different. Water content is also one of the factors that affect the resistivity value (Abidin et al., 2013). However, in this case, we can say that the water content was considered outliers. In addition, the water content affects the compaction process in reciprocal relations. Increasing compaction effort helps reduce air-filled voids and, therefore, decreases soil resistivity (Hassan and Toll, 2015). Plant roots help water to overcome the cavity under (Acosta et al., 2022).

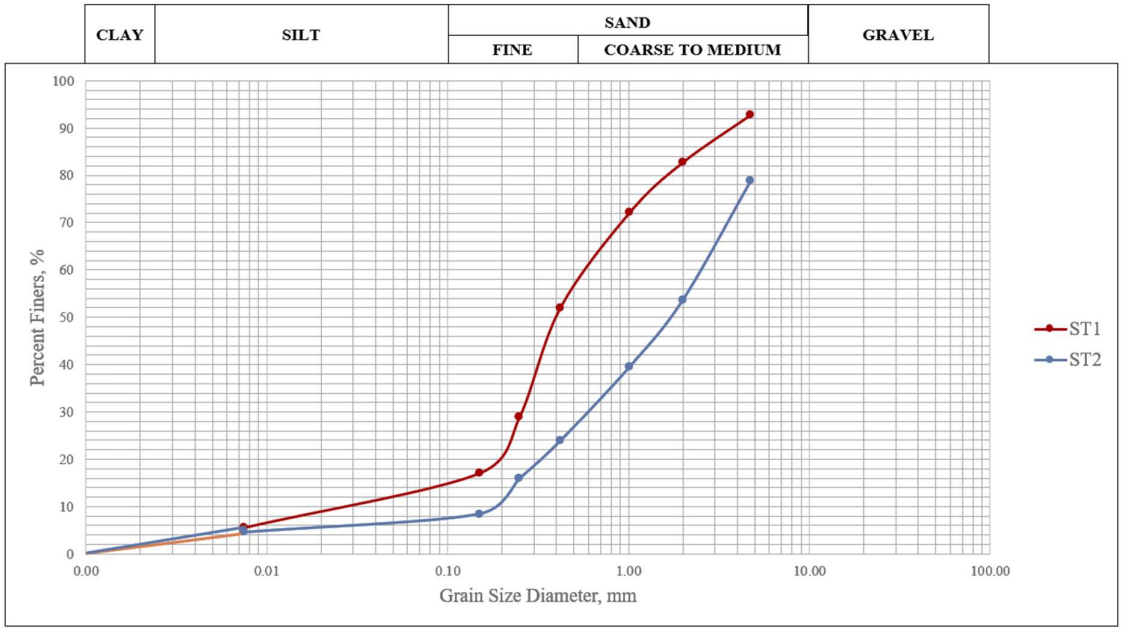

Figure 13. Graph of soil sieve analysis ST 1 and ST 2.

There are many gardens and rice fields in the study area. All samples had high moisture content (>25%) and showed decreased compaction. The water content breaks down in the rock causing cavities in the karst. These results indicate that the northern area has undergone the karstification process well so the cavity in the southern area is widening to the northern**.**

Direct shear strength analysis

The direct shear test obtained several parameters, i.e., the internal shear angle of the soil (ϕ), and cohesion (C). We then analyzed the relationship of some of these parameters to obtain the safety factor. From the examination, normal stress (s) and maximum shear stress were obtained, as shown in Table 2**.** The test results for both samples are shown in Figures 14 and15. Each sample was tested three times with normal stress of 10, 20, and 30 N, respectively. In general, the shear stress is lower, and therefore, the strain deformation is going lower too. As for the results of the pressure of 10, 20, and 30 N, respectively, they are represented by symbols ■, ▲, and ♦ and curves. As shown in Figure 14, the shear stress increases along with the increase of shear deformation of the ductile type. This circumstance indicates a contraction phase at higher normal stress followed by a dilatation phase. At standard normal stress, the boundary soil tends to flatten throughout the shear process (Yavari et al., 2016). Shear and normal stresses can be closely related to linear functions, with shear angles of 24° and cohesion values of 0.53 kg/cm^2. The experimental results using ST 2 sample are shown in Figure 15. Similar to the ST 1 sample, its behaviour is ductile. The behaviour of shear stress is similar to that shown in the previous figure. However, the maximum shear stress is less than the maximum shear stress in ST 1. Soil tends to make contraction in the first phase and then expands, and soil tends to expand from the beginning with low normal stress (Yavari et al., 2016). The shear angle is 45°, and the soil has a cohesion value of 0.124 kg/cm^2. These parameters from both samples indicate that the two extreme points' shear angle (ϕ) is loose or not solid. These measurements show excellent reproducibility in terms of shear stress and shear deformation. The relationship between shear and normal stress may be closely related to the linear function that determines the shear angles and cohesion.

Table 2. Normal stress and maximum shear stress.

Normal Stress					
σ_1 (kg/cm^2)		**σ_2 (kg/cm^2)**		**σ_3 (kg/cm^2)**	
ST 1	ST 2	ST 1	ST 2	ST 1	ST 2
0.320	0.320	0.640	0.640	0.960	0.960
Maximum Shear Stress (kg/cm^2)					
ST 1	ST 2	ST 1	ST 2	ST 1	ST 2
0.638	0.325	0.839	0.551	0.901	0.776

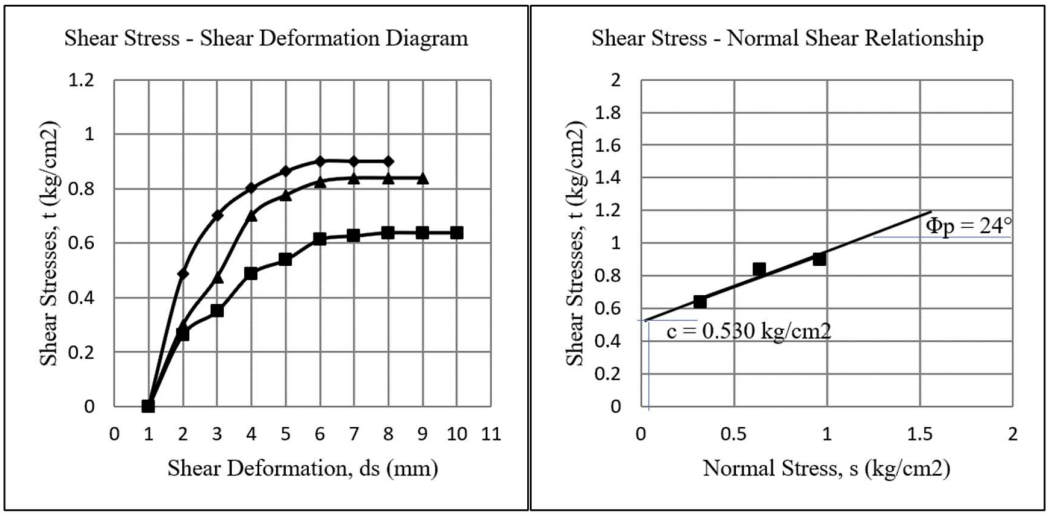

Figure 14. Shear strength curve of ST 1.

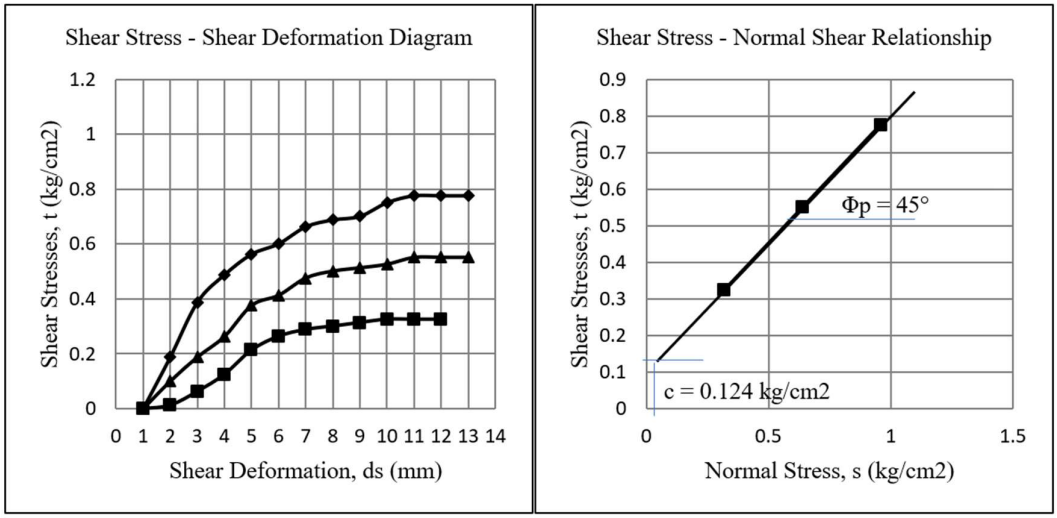

Figure 15. Shear strength curve of ST 2.

Both shear angles are larger than 20°. For the ST 1 sample, its value is less than 25°. The shear angle between 20°-25° indicates the intermediate level potential of landslides. More than 25° is located in the stable area (Sujit, 2015). The ST 2 sample is in this category. These results show that the research area has a stable slope when viewed using the shear angle value. However, an opposite interpretation would be obtained if it is based on a very low cohesion value. Cohesion values in the range of 0.1-0.9 have a high potential for landslides (Sujit, 2015). Both samples indicate that the research area has a high possibility of subsidence. Soil cohesion is influenced by the cementing material that firmly binds the soil particles together. This bond can be broken by water, which causes the material to collapse (Sujit, 2015). Previously, we explained that water activity could develop cavities in limestone (karst). This circumstance is very likely to occur as we reveal the caves distribution in the study area, especially in the southern part.

Join interpretation

Research has been carried out employing resistivity methods and geotechnical parameters. Based on the results of the resistivity method, the distribution of caves may be more dominant in the southern part of the study area. Samples for geotechnical research were taken from two points, which are considered to represent the northern and southern parts of the research area. We attempted to explain all the results and interpretations comprehensively in Table 3.

The northern part of the research area can be considered a stable area. This area has a resistivity value of 150-1600 Ωm, which is interpreted as massive limestone. The soil has a sandy size and is well-graded.

However, this area is increasingly insecure to be used as a residential area as indicated by reduced compaction due to the water influence. A very low cohesion value indicates the loosening state of the soil particle bonds, which would make this area unsafe, especially when the karstification process is going well. The results and interpretation of the shear angle also suggest that this area is prone to landslides. The southern part of the research area has a very high potential for a landslide. The overall results show similar results except for the shear angle. The shear angle results that show a stable area can be considered as outliers when compared to other results. The subsurface caves are characterized by very high resistivity values in this area (>4800 m). Grain size is a mixture of sand and gravel. The plant activity, especially root growth, can penetrate through the bonds of soil particles that carry water, which results in the decrease of its compaction. The cohesion value is also very low, so there is a high potential for the occurrence of landslides. This landslide can occur if the soil on the surface collapses into the cave.

Table 3. Recap of results and interpretation of resistivity and geotechnical parameters.

No	Parameter	Results (value)		Interpretation	
		Northern area	Southern area	Northern area	Southern area
1	Resistivity	150-1600 Ωm	>4800 Ωm	Massive limestone	Air-filled weathered limestone
2	Uniformity Coefficient (C_U)	4.192	15.725	Sandy limestone	Sand-gravel limestone
3	Curvature Coefficient (C_C)	1.216	0.923	Well-graded	Poor-graded
4	Water content	27.4%	33.6%	Decreased compaction	
5	Shear angle	24°	45°	Intermediate level potency of landslides	Stable area
6	Cohesion	0.53 kg/cm^2	0.124 kg/cm^2	High potency landslides	

Conclusion

The karstification process on limestone in the study area is going well with the presumed distribution of the dominating cave in the southern part of the research area. This indicates one factor of subsidence in this area. Very high resistivity values (>4800 Ωm) characterize the air in the limestone as cavities. Landslide potential was also found at this location based on the analysis of geotechnical parameters. The geotechnical parameters used were uniformity coefficient, curvature coefficient, water content, shear angle, and cohesion. The results of these parameters indicate that the entire area has a high potential for landslides, both in the southern and northern parts of the research area. This research has provided new insights for the society that the research area has a potential for land development. The methodological procedures in this study can also be used to investigate other areas in order to utilize karst area at an effective cost.

Acknowledgements

The authors would like to thank all parties who have contributed to the research. This research was supported by the Research and Community Service Institute (LPPM) of Hasanuddin University, and the Department of Geophysics, Faculty of Mathematics and Natural Sciences, Hasanuddin University.

References

Abd El Aal, A. 2017. Identification and characterization of near surface cavities in Tuwaiq Mountain Limestone, Riyadh, KSA, "detection and treatment." *Egyptian Journal of Petroleum* 26(1):215-223, doi:10.1016/j.ejpe.2016.04.004.

Abidin, M.H.B.Z., Wijeyesekera, D.C., Saad, R. and Ahmad, F. 2013. The influence of soil moisture content and grain size characteristics on its field electrical resistivity. *Electronic Journal of Geotechnical Engineering* 18 D(March):699-705.

Acosta, J.A., Gabarrón, M., Martínez-segura, M., Martínez-martínez, S., Faz, Á., Pérez-pastor, A., Gómez-lópez, M.D. and Zornoza, R. 2022. Soil water content prediction using Electrical Resistivity Tomography (ERT) in Mediterranean tree orchard soils. *Sensors* 22(4):1-13, doi:10.3390/s22041365.

Arisona, A., Ishola, K.S. and Nawawi, M.N.M. 2020. Subsurface void mapping using geophysical and geotechnical techniques with uncertainties estimation: case study of Kinta Valley, Perak, Malaysia. *Springer Nature Applied Sciences* 2(1171):1-12, doi:10.1007/s42452-020-2967-x.

Augie, A.I., Saleh, M., Ologe, O., Salako, K.A., Rafiu, A.A. and Yahaya, M. 2022. Correlation of 2D electrical resistivity and self-potential methods for the assessment of the integrity of Goronyo Dam NW Nigeria. *Chiang Mai University Journal of Natural Sciences* 21(3):e2022043, doi:10.12982/CMUJNS.2022.043.

Bakhshipour, Z., Huat, B.B.K., Ibrahim, S., Asadi, A. and Kura, N.U. 2013. Application of geophysical techniques for 3D geohazard mapping to delineate cavities and

potential sinkholes in the Northern Part of Kuala Lumpur, Malaysia. *The Scientific World Journal* 629476:1-11, doi:10.1155/2013/629476.

Baluch, K., Kim, J.G., Kim, J.G., Ko, Y.H., Jung, S.W. and Baluch, S.Q. 2022. Assessment of sinkholes investigations in Jangseong-Gun Area, South Korea, and recommendations for similar studies. *International Journal of Environmental Research and Public Health* 19(3):1111, doi:10.3390/ijerph19031111.

Chen, M.L., Wu, G.J., Gan, B.R., Jiang, W.H. and Zhou, J.W. 2018. Physical and compaction properties of granular materials with artificial grading behind the particle size distributions. *Advances in Materials Science and Engineering* 2018(8093571):1-20, doi:10.1155/2018/8093571.

Cortellazzo, G., Bellò, E., Busana, S. and Favaretti, M. 2021. Experimental acceptance procedure for using cullet in the gas collection layer of MSW landfill. *Indian Geotechnical Journal* 51(5):877-886, doi:10.1007/s40098-020-00472-w.

Das, B.M. 2021. *Principles of Geotechnical Engineering* (10th ed.). Cengage Learning. https://www.cengage.com/c/principles-of-geotechnical-engineering-10e-das/9780357420478PF

Ezersky, M.G., Legchenko, A., Eppelbaum, L. and Al-Zoubi, A. 2017. Overview of the geophysical studies in the dead sea coastal area related to evaporite karst and recent sinkhole development. *International Journal of Speleology* 46(2):277-302, doi:10.5038/1827-806X.46.2.2087.

Farooq, M., Park, S., Song, Y.S., Kim, J.H., Tariq, M. and Abraham, A.A. 2012. Subsurface cavity detection in a karst environment using Electrical Resistivity (ER): a case study from Yongweol-ri, South Korea. *Earth Sciences Research Journal* 16(1):75-82.

Figueroa-Miranda, S., Tuxpan-Vargas, J., Ramos-Leal, J.A., Hernández-Madrigal, V.M. and Villaseñor-Reyes, C.I. 2018. Land subsidence by groundwater over-exploitation from aquifers in tectonic valleys of Central Mexico: a review. *Engineering Geology* 246:91-106, doi:10.1016/j.enggeo.2018.09.023.

García-Soriano, D., Quesada-Román, A. and Zamorano-Orozco, J.J. 2020. Geomorphological hazards susceptibility in high-density urban areas: a case study of Mexico City. *Journal of South American Earth Sciences* 102(102667):1-11, doi:10.1016/j.jsames.2020.102667.

Hassan, A.A. and Toll, D.G. 2015. Water content characteristics of mechanically compacted clay soil determined using the electrical resistivity method. *ICE Proceedings of the XVI ECSMGE Geotechnical Engineering for Infrastructure and Development,* ISBN 978-0-7277-6067-8, 793-798, doi:10.1680/ecsmge.60678.

Ikuemonisan, F.E. and Ozebo, V.C. 2020. Characterization and mapping of land subsidence based on geodetic observations in Lagos, Nigeria. *Geodesy and Geodynamics* 11(2):151-162, doi:10.1016/j.geog.2019.12.006.

Imran, A.M., Farida, M., Arifin, M.F., Husain, R. and Hafidz, A. 2016. Coral reef development as an indicator of seal level fluctuation: a preliminary study on Pleistocene reef in Bulukumba, South Sulawesi. *Indonesian Journal on Geoscience* 3(1):53-66, doi:10.17014/ijog.3.1.53-66.

Massinai, M.A. and Massinai, M.F.I. 2018. Determination hypocentre and focal mechanism earthquake of Oct 31, 2016 in Bone, South Sulawesi. *Journal of Physics: Conference Series* 979(012045):1-5, doi:10.1088/1742-6596/979/1/012045.

Massinai, M.A., Massinai, M.F.I., Kurniati, A. and Syamsuddin, E. 2019. Identification fault characteristic in Southern Sulawesi by focal mechanism. *Journal of Physics: Conference Series* 1363(012040):1-7, doi:10.1088/1742-6596/1363/1/012040.

Massinai, M.A., Sudradjat, A. and Lantu, L. 2014. The influence of seismic activity in South Sulawesi Area to the geomorphology of Jeneberang watershed. *International Journal of Engineering and Technology* 3(10):945-948.

O'Kelly, B.C. and Nogal, M. 2020. Determination of soil permeability coefficient following an updated grading entropy method. *Geotechnical Research* 7(1):58-70, doi:10.1680/jgere.19.00036.

Oyeyemi, K.D., Aizebeokhai, A.P., Adagunodo, T.A., Olofinnade, O.M., Sanuade, O.A. and Olaojo, A.A. 2017. Subsoil characterization using geoelectrical and geotechnical investigations: implications for foundation studies. *International Journal of Civil Engineering and Technology* 8(10):302-314.

Pusparini, W., Ilmi, N.N. and Sunardi, E. 2019. Determining maturity rate of hydrocarbon using sample core from geochemistry survey in Padamarang Sub-Basin, Bone Gulf, South of Sulawesi. *Journal of Geological Sciences and Applied Geology* 3(1):1-5.

Sari, N.D.P., Massinai, M.F.I., Hasan, A., Rahayu, D. and Nurdin, N.H. 2019. Subsurface prediction using resistivity method (case study: Bira, South Sulawesi, Indonesia). *Journal of Physics: Conference Series* 1341(082028):1-5, doi:10.1088/1742-6596/1341/8/082028.

Sujit, M. 2015. Assessing cohesion, friction angle and slope instability in the Shivkhola watershed of Darjiling Himalaya. *International Research Journal of Earth Sciences* 3(8):1-10.

Wichtmann, T. and Triantafyllidis, T. 2013. Effect of uniformity coefficient on G/Gmax and damping ratio of uniform to well-graded quartz sands. *Journal of Geotechnical and Geoenvironmental Engineering* 139(1):59-72, doi:10.1061/(asce)gt.1943-5606.0000735.

Wilopo, W., Putra, D.P., Fathani, T.F., Widodo, S., Pratama, G.N.I.P., Nugroho, M.S. and Prihadi, W.R. 2022. Identification of subsidence hazard zone by integrating engineering geological mapping and electrical resistivity tomography in Gunung Kidul Karst Area, Indonesia. *Journal of Degraded and Mining Lands Management* 9(2):3281-3291, doi:10.15243/jdmlm.2022.092.3281.

Yavari, N., Tang, A.M., Pereira, J.-M. and Hassen, G. 2016. Effect of temperature on the shear strength of soils and the soil–structure interface. *Canadian Geotechnical Journal* 53(7):1186-1194, doi:10.1139/cgj-2015-0355.

Zhou, W., Beck, B.F. and Adams, A.L. 2002. Effective electrode array in mapping karst hazards in electrical resistivity tomography. *Environmental Geology* 42(8):922-928, doi:10.1007/s00254-002-0594-z